Experimental implementation of reverse time migration for nondestructive evaluation applications

Brian E. Anderson[a)]
Acoustics Research Group, Department of Physics and Astronomy, Brigham Young University, N283 Eyring Science Center, Provo, Utah 84602
bea@byu.edu

Michele Griffa
Laboratory for Building Science and Technology, EMPA, Swiss Federal Laboratories for Materials Science and Technology, CH-8600, Dübendorf, Switzerland
michele.griffa@empa.ch

Pierre-Yves Le Bas, Timothy J. Ulrich, and Paul A. Johnson
Solid Earth Geophysics Group (EES-17), Los Alamos National Laboratory, MS D443, Los Alamos, New Mexico 87545
pylb@lanl.gov, tju@lanl.gov

Abstract: Reverse time migration (RTM) is a commonly employed imaging technique in seismic applications (e.g., to image reservoirs of oil). Its standard implementation cannot account for multiple scattering/reverberation. For this reason it has not yet found application in nondestructive evaluation (NDE). This paper applies RTM imaging to NDE applications in bounded samples, where reverberation is always present. This paper presents a fully experimental implementation of RTM, whereas in seismic applications, only part of the procedure is done experimentally. A modified RTM imaging condition is able to localize scatterers and locations of disbonding. Experiments are conducted on aluminum samples with controlled scatterers.

PACS numbers: 43.35.Zc, 43.40.Le, 43.60.Tj [CG]
Date Received: September 30, 2010 **Date Accepted:** November 17, 2010

1. Introduction

For many years, geophysicists have used reverse time migration (RTM) to image below the Earth's surface.[1–9] The RTM imaging technique employs forward and backward propagation phases as does the standard implementation of time reversal.[10–12] The forward propagation phase of traditional RTM imaging in seismic applications utilizes a source that injects wave energy into the Earth while multiple receiver transducers are used to collect the reflected signals from scatterers of interest in the Earth. A numerical model of the subsurface region of the Earth where the experiment was conducted is then used to compute forward and backward propagation wave fields used in the imaging condition. The numerical model is based upon some necessary and simplifying assumptions, e.g., a certain degree of homogeneity of the propagation medium. Indeed, the scatterers' locations are not known in advance and are the targets of the imaging procedure. The forward propagation is simulated in the model with the same source waveform used in the experiment and the wave field in the region of interest (ROI) is computed. The signals recorded experimentally by the receiver transducers are reversed in time and used as the sources for the backward propagation simulation. The wave field is then

[a)]Author to whom correspondence should be addressed.

numerically recorded at the same points in the ROI for both forward and backward propagation simulations. A zero-lag cross-correlation of the forward and backward propagation wave fields, known as an imaging condition, is computed at each ROI point to form the image. A key limitation of traditional RTM imaging consists in the initial model assumptions: reverberation due to the actual finite size of the propagation domain and/or multiple scattering by the actual medium structure is usually encoded in the experimentally acquired signals and corrupts the quality of the image. Significant efforts have been dedicated in the fields of seismology and seismic imaging to cope with this intrinsic limitation. Useful approaches consist either in trying to filter out part of the reverberation/multiple scattering contributions to the experimental signals before using them for the backward propagation stage, with consequent limitations in which types of scatterers can be imaged,[13] or in removing from the formed image the corresponding artifacts after their classification and detection.[14] A further approach focuses on developing imaging conditions that take partially into account the reverberation/multiple scattering processes.[15] However, the complete exploitation of reverberation/multiple scattering in RTM imaging conditions still remains an open challenge.

Laboratory scale applications of RTM for sound/ultrasound imaging and inspection are inevitably affected by the types of limitations noted above. Indeed, reverberation is almost always unavoidable. Lin and Yuan[16–18] extended the application of RTM to nondestructive testing. Their experiments were conducted on an aluminum plate and followed the traditional RTM procedure utilizing a single reflection from the scatterer(s) of interest. Thus they computed the forward and backward propagation wave fields numerically with a model of the sample. The technique they presented could be extended to imaging of defects within a three dimensional sample. However, their sample needed to be large to avoid reverberation by applying appropriate time windowing of their signals. The difficulty with traditional RTM imaging of samples for nondestructive evaluation, as done by Lin and Yuan, is that the samples are often quite small and may have complex geometries giving rise to multiple scattering/reverberation and making a single scattered wave from a scatterer of interest difficult to distinguish in time.

In this paper we present a fully experimental implementation of RTM imaging where the forward and backward propagation wave fields are measured with a scanning laser vibrometer. Because we do not compute the wave field inside the sample under test, the proposed fully experimental RTM imaging technique is limited in application to surface features, near surface features (within an approximate half-wavelength acoustic penetration depth), features on the other side of a thin plate, and features embedded between two thin laminated plates. The experiments conducted in the paper investigate the third application area to show that objects located on the other side of a thin plate may be imaged even when that side is not physically accessible. We include multiple reflections in our recorded wave fields as is commonly done with standard time reversal, where multiple scattering actually enhances the imaging spatial resolution. As with time reversal techniques, RTM is limited in its spatial resolution by the diffraction limit (in the present case it is a half wavelength for the guided, bending wave in the plate). Time reversal may be used to image linear scatterers through a series of time reversal experiments and complex processing,[19,20] or it may be used to directly image nonlinear scatterers (which are the sources of new frequency content).[21–24] However, the typical aim of time reversal is to localize sources,[25–30] whereas the aim of RTM is to directly image linear scatterers without the need for complex processing, or the requirement that the scatterers be nonlinear.

2. Method

Figure 1(a) depicts an illustration of a typical sample to be inspected by RTM. A source transducer S emits a sinusoidal pulse of energy such as that shown in Fig. 1(b). The source pulse used in the experiments consisted of a 200 kHz pulse that was modulated by a sine squared envelope. As the wave energy traverses the medium, a laser

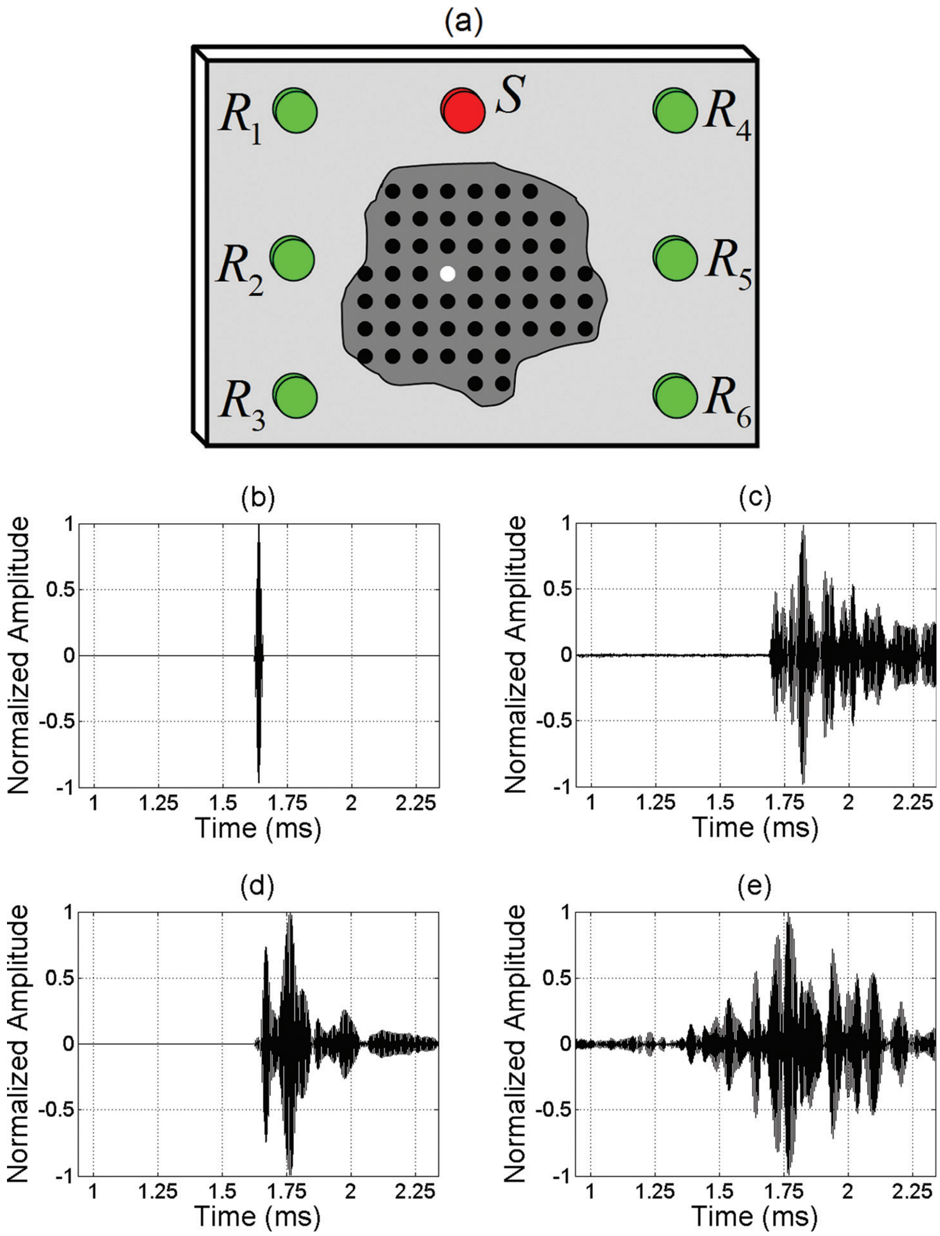

Fig. 1. (Color online) (a) Schematic illustration of a sample under test. S is the illumination source. R_i are the transceivers constituting the TRM. A scanning laser vibrometry grid is defined on the sample surface opposite to the one where R_i are located. (b) Sample source waveform input by the source transducer. (c) Sample waveform detected by the laser vibrometer during forward propagation. (d) Sample waveform recorded by a receiver transducer, which is then time reversed and used as the source of the backward propagation. (e) Sample waveform detected by the laser vibrometer during the backward propagation stage, at the same location as for (c).

vibrometer detects the out of plane velocity signals [sample waveform shown in Fig. 1(c) for the white colored point] at various points of a scanning grid in the ROI, denoted by the black dots in Fig. 1(a). These temporal signals form the three dimensional forward propagation matrix, $F_{x,y}(t)$, consist of spatial dimensions x and y and with time as the third dimension. This experiment is repeated many times at each point in the ROI to improve the signal to noise ratio through averaging. The forward propagation is also recorded [sample waveform shown in Fig. 1(d)] at one or more receiver transducers, R_i, which form a time reversal mirror (TRM).[10–12] The signals recorded by the TRM are then time reversed and emitted from the respective transducers in the TRM itself, now acting as sources. During this backward propagation phase, a laser vibrometer is again used to detect the out of plane vibration velocity at the same points in the ROI [sample waveform shown in Fig. 1(e) for the white colored point]. These temporal signals form the three dimensional backward propagation matrix, $B_{x,y}(t)$.

As one may observe from Figs. 1(c) and 1(e), the individual reflections off scatterers and/or sample boundaries are indistinguishable within the time window and frequency bandwidth utilized. Thus the traditional RTM imaging method cannot be used. Instead we propose that the multiple reflections be exploited to take advantage of the repeated focusing on scatterers. The imaging condition that we propose departs from the traditionally used imaging condition, $I_{x,y}$,[31]

$$I_{x,y} = \left| \Im^{-1}\left\{ \sum_{f_L}^{f_U} \Im\left(F_{x,y}\right)\Im\left(B_{x,y}\right) \right\} \right|, \tag{1}$$

where $\Im$ represents the Fourier transform, f_L represents the lowest frequency in the band of interest, and f_U represents the highest frequency in the band of interest. Here we propose to sum the magnitudes of the Fourier transform components rather than to sum the complex Fourier transform components and then take the magnitude. This modified imaging condition, $M_{x,y}$, is computed as follows:

$$M_{x,y} = \Im^{-1}\left\{ \sum_{f_L}^{f_U} \left|\Im\left(F_{x,y}\right)\Im\left(B_{x,y}\right)\right| \right\}. \tag{2}$$

This modified imaging condition effectively removes the effects of interference due to the multiple scattering. Further work is underway to fully explore the merits of this modified imaging condition.

3. Experiment

A hexagonal steel nut was glued (with Super Glue®) onto an aluminum plate to demonstrate a fully experimental RTM imaging process in a highly scatterering medium. The aluminum plate measured 0.84 mm × 152 mm × 195 mm in size. The wave field in the plate is dominated by dispersive transverse bending waves,[32] due to the plate thickness and mode conversion, with wave speed, c_B, governed by

$$c_B = \left(\omega^2 \frac{Eh^2}{12\rho(1-\sigma^2)}\right)^{1/4}, \tag{3}$$

where ω is the angular frequency, E is the Young's modulus of elasticity, ρ is the bulk density, and σ is the Poisson's ratio. Equation (3) yields a value of approximately 1300 m/s (assuming $E = 71$ GPa, $\rho = 2700$ kg/m^3, and $\sigma = 0.33$). Seven 13 mm diameter, 2 mm thickness compressional piezoelectric transducers were glued onto the plate at distributed random locations. One of the transducers was utilized as a source and the other six comprised the TRM (as with time reversal, a higher number of TRM elements would improve the quality of RTM results). The source waveform is a sinusoidal pulse with a center frequency of 200 kHz, and a pulse length of 40 μs (central frequency wavelength is 6.5 mm, and frequency bandwidth is 100 kHz). The RTM procedure illustrated in Fig. 1 was carried out and the imaging condition given in Eq. (2) was computed for each point in the ROI (the ROI was just large enough to

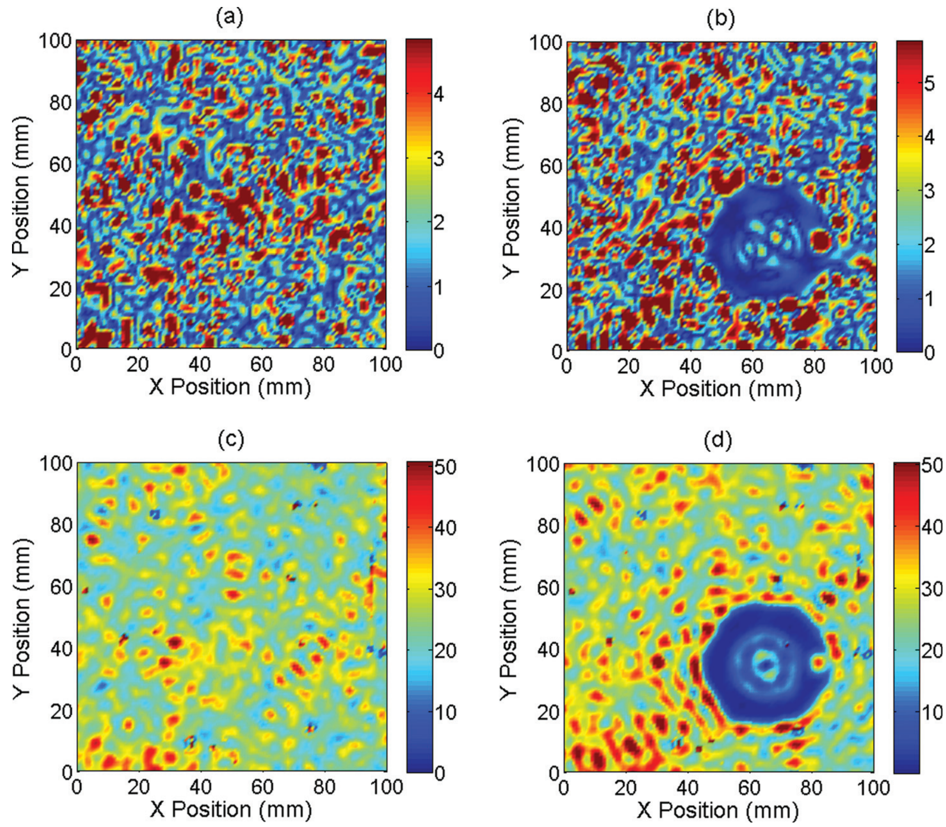

Fig. 2. (Color online) RTM images of a thin aluminum plate without and with a steel nut glued on using the standard and modified imaging conditions, $I_{x,y}$ and $M_{x,y}$, respectively. (a) $I_{x,y}$ without the nut. (b) $I_{x,y}$ with the nut. (c) $M_{x,y}$ without the nut. (d) $M_{x,y}$ with the nut. The amplitudes in these figures are individually scaled such that the average amplitude in the square region spanning ($x = 0$–40 mm and $y = 60$–100 mm) corresponds to a color of green, while zero corresponds to a dark blue color and twice the average amplitude corresponds to a dark red color.

include the nut). The laser vibrometer scanned the side of the plate opposite to the nut.

Figure 2 contains plots of the $I_{x,y}$ and $M_{x,y}$ images both without and with the nut glued to the plate. Figures 2(a) and 2(b) display $I_{x,y}$ without and with the nut, respectively. Figures 2(c) and 2(d) display $M_{x,y}$ without and with the nut, respectively. The points directly opposite of the nut are clear minima in the image. The reason for the local maxima at $x = 82$ mm, and $y = 35$–36 mm in Fig. 2(d) is unclear but may be due to speckle noise detected by the laser vibrometer due to an imperfect reflecting surface, or it may be a local disbonding region. Note the clear difference in amplitude between Figs. 2(a) and 2(b) and between Figs. 2(c) and 2(d) when the nut is present. Further, note the improvement of the image quality found in Fig. 2(d) relative to Fig. 2(b) in terms of the clear color contrast. The amplitude of the image without the nut is more uniform in Fig. 2(c) than in Fig. 2(a). We conclude that the $M_{x,y}$ images allow for easier detection of scatterers than the $I_{x,y}$ images.

An additional experiment was conducted to determine whether $M_{x,y}$ could distinguish points of imperfect bonding. A second hexagonal steel nut was glued onto the plate with two locations not having the same amount of glue. Figure 3(a) displays a photograph of the second nut removed from the plate after the experiment was completed. Note the two locations, denoted by red arrows, where there was insufficient glue. The experimental procedure used to obtain the $M_{x,y}$ images in Fig. 2 is used to image the partially disbonded nut. Figure 3(b) displays the $M_{x,y}$ image. The two

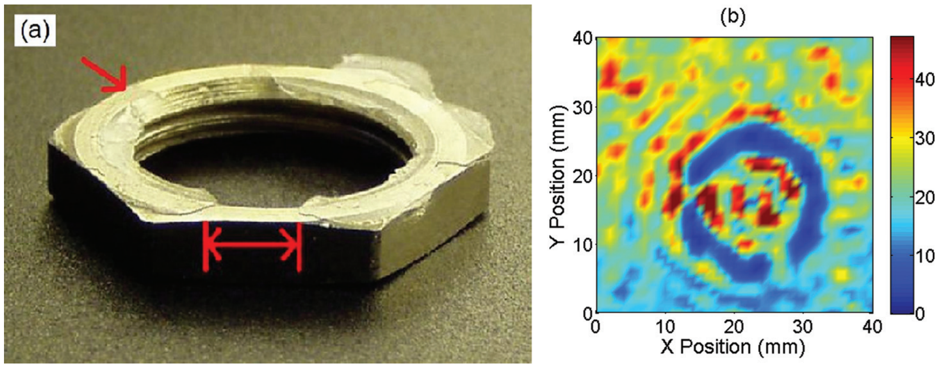

Fig. 3. (Color online) (a) Photograph of the second steel nut that was imperfectly bonded to a thin aluminum plate. (b) RTM image (modified imaging condition, $M_{x,y}$) of the nut (imaged from the other side of the plate).

disbonding locations are visible in the $M_{x,y}$ image at $x = 14$ mm and $y = 17$ mm, and at $x = 26$ mm and $y = 9$ mm and match the locations indicated in the photograph.

There is a finite amount of speckle noise in the RTM images as well, for example, the peak at $x = 82$ mm and $y = 35$ mm. The speckle noise shows up as local maxima and minima, yet the minima rarely approach the magnitude of the minima when a nut is imaged. Speckle noise does limit the imaging capacity of RTM, and further work could focus on quantifying this limit.

4. Conclusion

It has been shown that RTM imaging may be applied to the case where multiple reflections are included in the imaging condition. This work presents a fully experimental implementation of RTM imaging. The modified imaging condition [Eq. (2)] proposed in this work allows scatterers to be distinguished better than the standard imaging condition [Eq. (1)] does. The reason for the better performance of the modified imaging condition is currently unknown but is the subject of ongoing research. The performance of these imaging methods as a function of the number of TRM elements, length of time used to record at the TRM, spatial distribution of the TRM, and frequency bandwidth of the source is the subject of ongoing research as well. One may use this technique to locate scatterers on the other side of a thin plate. Additionally, one may locate regions of imperfect bonding for nondestructive testing applications. A more in depth analysis of the quality of the RTM image as compared to other time reversal imaging conditions is currently underway.

Acknowledgments

This research was supported by institutional support [Laboratory Directed Research and Development (LDRD)] at the Los Alamos National Laboratory. The authors are grateful for the assistance and insight provided by Huseyin Denli, Lianjie Huang, Robert Guyer, Carène Larmat, and Jim TenCate.

References and links

[1]J. F. Claerbout, "Toward a unified theory of reflector mapping," Geophysics **36**(3), 467–481 (1971).
[2]E. Baysal, D. Kosloff, and J. W. C. Sherwood, "Reverse time migration," Geophysics **48**(11), 1514–1524 (1983).
[3]S. A. Levin, "Principle of reverse-time migration," Geophysics **49**(5), 581–583 (1984).
[4]W.-F. Chang and G. A. McMechan, "Reverse-time migration of offset vertical seismic profiling data using the excitation-time imaging condition," Geophysics **51**(1), 67–84 (1986).
[5]W.-F. Chang and G. A. McMechan, "Elastic reverse-time migration," Geophysics **52**(10), 1365–1375 (1987).
[6]W.-F. Chang and G. A. McMechan, "3-D acoustic prestack reverse-time migration," Geophys. Prospect. **38**(7), 737–755 (1990).

[7]W.-F. Chang and G. A. McMechan, “3-D elastic prestack, reverse-time depth migration,” Geophysics **59**(4), 597–609 (1994).
[8]R. Sun and G. A. McMechan, “Scalar reverse-time depth migration of prestack elastic seismic data,” Geophysics **66**(5), 1519–1527 (2001).
[9]S. Chattopadhyay and G. A. McMechan, “Imaging conditions for prestack reverse-time migration,” Geophysics **73**(3), S81–S89 (2008).
[10]M. Fink, “Time reversed acoustics,” Phys. Today **50**(3), 34–40 (1997).
[11]B. E. Anderson, M. Griffa, C. Larmat, T. J. Ulrich, and P. A. Johnson, “Time reversal,” Acoust. Today **4**(1), 5–16 (2008).
[12]C. Larmat, R. A. Guyer, and P. A. Johnson, “Time-reversal methods in geophysics,” Phys. Today **63**(8), 31–35 (2010).
[13]A. B. Weglein, “Multiple attenuation: An overview of recent advances and the road ahead,” The Leading Edge **18**, 40–44 (1999).
[14]A. Guitton, B. Kaelin, and B. Biondi, “Least-squares attenuation of reverse-time migration artifacts,” Geophysics **72**(1), S19–S23 (2007).
[15]A. E. Malcolm, B. Ursin, and M. V. de Hoop, “Seismic imaging and illumination with internal multiples,” Geophys. J. Int. **176**, 847–864 (2009).
[16]X. Lin and F. G. Yuan, “Damage detection of a plate using migration technique,” J. Intell. Mater. Syst. Struct. **12**(7), 469–482 (2001).
[17]X. Lin and F. G. Yuan, “Detection of multiple damages by prestack reverse-time migration,” AIAA J. **39**(11), 2206–2215 (2001).
[18]X. Lin and F. G. Yuan, “Experimental study applying a migration technique in structural health monitoring,” Struct. Health Monit. Int. J. **4**(4), 341–353 (2005).
[19]J.-L. Robert and M. Fink, “Spatio-temporal invariants of the time reversal operator,” J. Acoust. Soc. Am. **127**(5), 2904–2912 (2010).
[20]J.-L. Robert and M. Fink, “The prolate spheroidal wave functions as invariants of the time reversal operator for an extended scatterer in the Fraunhofer approximation,” J. Acoust. Soc. Am. **125**(1), 218–226 (2009).
[21]T. J. Ulrich, P. A. Johnson, and A. Sutin, “Imaging nonlinear scatterers applying the time reversal mirror,” J. Acoust. Soc. Am. **119**(3), 1514–1518 (2006).
[22]T. J. Ulrich, P. A. Johnson, and R. A. Guyer, “Interaction dynamics of elastic waves with a complex nonlinear scatterer through the use of a time reversal mirror,” Phys. Rev. Lett. **98**(10), 104301 (2007).
[23]T. J. Ulrich, A. M. Sutin, T. Claytor, P. Papin, P.-Y. Le Bas, and J. A. TenCate, “The time reversed elastic nonlinearity diagnostic applied to evaluation of diffusion bonds,” Appl. Phys. Lett. **93**(15), 151914 (2008).
[24]T. J. Ulrich, K. Van Den Abeele, P.-Y. Le Bas, M. Griffa, B. E. Anderson, and R. A. Guyer, “Three component time reversal: Focusing vector components using a scalar source,” J. Appl. Phys. **106**(11), 113504 (2009).
[25]M. Griffa, B. E. Anderson, R. A. Guyer, T. J. Ulrich, and P. A. Johnson, “Investigation of the robustness of time reversal acoustics in solid media through the reconstruction of temporally symmetric sources,” J. Phys. D: Appl. Phys. **41**, 085415 (2008).
[26]M. Scalerandi, A. S. Gliozzi, B. E. Anderson, M. Griffa, P. A. Johnson, and T. J. Ulrich, “Selective source reduction to identify masked sources using time reversal acoustics,” J. Phys. D: Appl. Phys. **41**, 155504 (2008).
[27]B. E. Anderson, T. J. Ulrich, M. Griffa, P.-Y. Le Bas, M. Scalerandi, A. S. Gliozzi, and P. A. Johnson, “Experimentally identifying masked sources applying time reversal with the selective source reduction method,” J. Appl. Phys. **105**(8), 083506 (2009).
[28]B. E. Anderson, R. A. Guyer, T. J. Ulrich, and P. A. Johnson, “Time reversal of continuous-wave, steady-state signals in elastic media,” Appl. Phys. Lett. **94**(11), 111908 (2009).
[29]D. Mennitt and M. Johnson, “Multiple-array passive acoustic source localization in urban environments,” J. Acoust. Soc. Am. **127**(5), 2932–2942 (2010).
[30]J. Sadler, K. Shapoori, and E. Malyarenko, “Locating an acoustic point source scattered by a skull phantom via time reversal matched filtering,” J. Acoust. Soc. Am. **128**(4), 1812–1822 (2010).
[31]P. Sava and S. Hill, “Overview and classification of wave field seismic imaging methods,” The Leading Edge **28**, 170–183 (2009).
[32]F. Fahy and P. Gardonio, *Sound and Structural Vibration, Radiation, Transmission and Response*, 2nd ed. (Academic, Oxford, 2007), Section 1.7, pp. 23–24.